Ocean Waves Measurement and Analysis, Fifth International Symposium WAVES 2005, 3rd-7th, July, 2005. Madrid, Spain
Paper number: 121

MODELLING OF WAVE DRIVEN SEDIMENT TRANSPORT OVER A PARTIALLY BURIED CYLINDER

Richard W. Gilbert[1], Emily A. Zedler[2],
Stéphan T. Grilli, M.ASCE, [1] and Robert L. Street, M.ASCE [2]

Abstract: A numerical wave tank (NWT), solving Fully Nonlinear Potential Flow equations, is used to drive Navier-Stokes (NS) simulations of wave-induced flow and sediment transport (both bed- and suspended load) around partially buried obstacles. Turbulence is represented in the NS model by Large Eddy Simulation (LES). The NS-LES model domain is initialized with the velocity fields computed in the NWT. For later time, the NS-LES model is driven by the NWT pressure gradient fields. Incident waves specified in the NWT can be arbitrary; here, only cases with periodic waves are presented. We discuss wave induced boundary-layer flows simulated in the coupled model. Examples of flow and sediment transport around partially buried cylinders are presented.

INTRODUCTION

In this work, we model wave-induced flows and sediment transport around partially buried cylinders, using a coupled wave-hydrodynamic-sediment transport model. While most similar work to date has usually been based on specifying a simple oscillatory flow to force the sediment transport (Zedler and Street 2005; Barr et al. 2004; Chang and Scotti 1991), here, we use the more realistic background wave velocity field created by fully nonlinear waves; we consider both waves propagating over flat bottom and shoaling over slopes. Our approach is consistent with earlier research, showing that nonlinear effects in shoaling wave fields yield asymmetric wave shapes and near-bottom currents, that strongly affect sediment transport and the resulting scouring/burial of bottom obstacles (Voropayev et al. 1999; Voropayev et al. 2003a). When approaching shore, due to refraction, shoaling ocean swells often become locally two-dimensional (2D) in the cross-shore direction. A 2D wave-form is thus a good approximation for simulating wave-induced sediment transport in an essentially cross-shore direction (e.g., Fig. 1). Recent laboratory experiments performed in a wave-tank with moving bed at Arizona State University (ASU; (Voropayev et al. 1999; Voropayev et al. 2003a; Voropayev et al. 2003b; Grilli et al. 2003; Grilli et al. 2004) show that small scale disturbances in the bottom topography, as compared to the wavelength, such as sand

[1]Graduate student and distinguished Professor and Chair, respectively, at the University of Rhode Island, Depart. of Ocean Engng., Narragansett, RI 02882, grilli@oce.uri.edu.

[2]Graduate student and Professor, respectively, at the Environmental Fluid Mech. Lab., Depart. of Civil & Env. Engng., Stanford University, Stanford, CA 94305, street@stanford.edu.

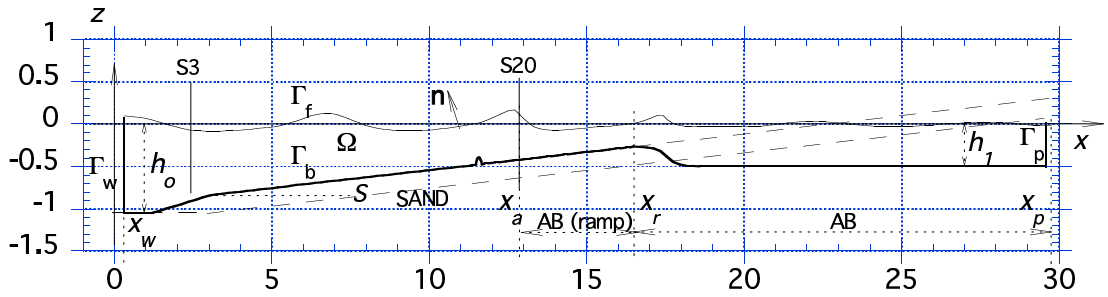

Fig. 1. 2D-NWT set-up for simulating ASU experiments of periodic wave shoaling and breaking over a sandy slope $S = 1 : 24$, with a 75% buried cylinder at $x = 12.8$.

ripples or small partially buried obstacles, usually affect flow velocities only within 2-3 significant diameters of the object and have negligible effects on the waveform. This allows us to simulate 2D wave "far-fields", to provide background wave velocities for driving the three-dimensional (3D) turbulent flow around bottom obstacles, in the "near-field".

We model far-field incident waves in a 2D Numerical Wave Tank (NWT) solving Fully Nonlinear Potential Flow (FNPF) equations, based on a higher-order Boundary Element Method (BEM) and an explicit time stepping. This NWT has been shown in earlier work to be very accurate for simulating both the shape and velocities of shoaling waves, as compared to laboratory measurements (Grilli and Subramanya 1996; Grilli and Horrillo 1999; Grilli et al. 2003). Fig. 1, for instance, shows the set-up of a recent comparison of NWT simulations with ASU's experiments (Grilli et al. 2003; Grilli et al. 2004). Fig. 2 shows that the simulated period averaged wave elevation and the near bottom horizontal velocity at 0.1 m above the bottom, are in good agreement with measurements at gage S20, close to breaking. Here, the NWT is similarly used to model velocities and pressure fields induced by nonlinear waves, and serve as forcing for a *near-field* nested Navier-Stokes (NS) model (Zedler and Street 2001; Zedler and Street 2002). At this time, no feed-back of NS model results into the NWT is implemented. This so-called "weak coupling" approach was successfully applied, in earlier work, to the modeling of shoaling, breaking, and post-breaking waves, in coupled 2D- and 3D-FNPD-NWTs and NS models (Guignard et al. 1999; Biausser et al. 2004). Periodic waves are generated in the NWT with a numerical wavemaker, as in the laboratory experiments. An absorbing beach (AB) is specified at the other extremity of the NWT, to dissipate incident wave energy before wave overturning and breaking occur Grilli and Horrillo 1997; Fig. 1). In the NS model, resolved-scale turbulence, which accounts for a majority of sediment transport, is represented by Large Eddy Simulations (LES). Sub-grid scale turbulence is represented by an eddy viscosity model. In the sediment transport module, bed-level sediment concentrations are obtained from vanRijn (1984b) formula, and suspended sediment transport is simulated with an advection-diffusion scheme. NWT simulations are 2D, but the NS-LES model simulations are fully 3D within a smaller computational domain located over the bottom area of interest (Fig. 3a), where wave-induced sediment transport is calculated.

An overview of governing equations and numerical methods for the NWT, NS-LES, and sediment transport models, is given in the next section. We then illustrate our coupled modeling approach, by generating 2D periodic waves over a flat bottom and driving sediment transport in the 3D near-field NS-LES domain, around a 75% buried cylindrical object. Results are given for the generated wave fields and sediment concentrations.

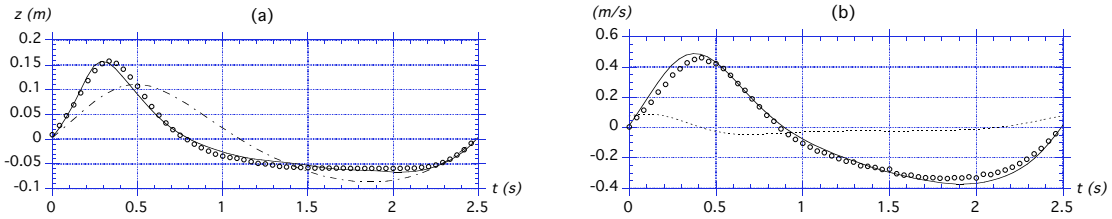

Fig. 2. NWT vs. ASU experiments (○) (S20, Fig. 1) : (a) wave elevation ((— - —) is S3); (b) horiz. u (——) and vert. w (- - - - -), velocities at 0.1 m above bottom.

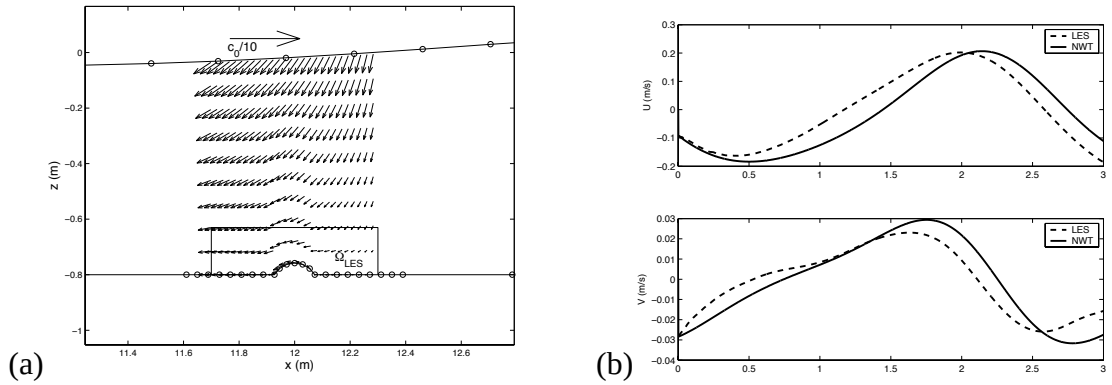

Fig. 3. Coupled NWT-NS-LES model for periodic waves : (a) typical velocity forcing in NWT and NS-LES domain $\Omega_{\rm LES}$; (b) velocities at (x = 11.7 m and z = −0.63 m).

BACKGROUND OF NUMERICAL MODELS

NWT Equations and Boundary Conditions

Equations for the 2D-NWT are briefly presented in the following (see Grilli and Subramanya 1996; Grilli and Horrillo 1997; Grilli et al. 2003, for details). The velocity potential $\phi(\boldsymbol{x},t)$ is introduced to describe the irrotational motion of an incompressible, inviscid fluid, in the vertical plane (x,z), and the velocity is defined by, $\boldsymbol{u} = \boldsymbol{\nabla}\phi = (u,w)$. Continuity equation in the fluid domain $\Omega(t)$ with boundary $\Gamma(t)$ is a Laplace's equation for the potential, $\nabla^2\phi = 0$ (Fig. 1), which is expressed as the Boundary Integral Equation (BIE),

$$\alpha(\boldsymbol{x}_l)\,\phi(\boldsymbol{x}_l) = \int_\Gamma \left\{ \frac{\partial\phi}{\partial n}\,G - \phi\,\frac{\partial G}{\partial n} \right\} d\Gamma \tag{1}$$

where the Green's functions are defined as,

$$G(\boldsymbol{x},\boldsymbol{x}_l) = -\frac{1}{2\pi}\log r \quad ; \quad \frac{\partial G}{\partial n} = -\frac{\boldsymbol{r}\cdot\boldsymbol{n}}{2\pi\, r^2} \tag{2}$$

with $\boldsymbol{r} = \boldsymbol{x} - \boldsymbol{x}_l$, $r = \mid \boldsymbol{r} \mid$, $\boldsymbol{x} = (x,z)$ and $\boldsymbol{x}_l = (x_l, z_l)$ position vectors for points on the boundary, $\boldsymbol{n} = (n_x, n_z)$ the outward unit normal vector to the boundary, and $\alpha(\boldsymbol{x}_l)$ is a geometric coefficient function of the exterior angle of the boundary at $\boldsymbol{x}_l$.

On the free surface Γ_f, ϕ satisfies the kinematic and dynamic boundary conditions,

$$\frac{D\,\boldsymbol{R}}{D\,t} = \left(\frac{\partial}{\partial t} + \boldsymbol{u}\cdot\boldsymbol{\nabla}\right)\boldsymbol{R} = \boldsymbol{\nabla}\phi \quad ; \quad \frac{D\phi}{Dt} = -gz + \frac{1}{2}\boldsymbol{\nabla}\phi\cdot\boldsymbol{\nabla}\phi - \frac{p_f}{\rho} \quad \text{on } \Gamma_f(t) \tag{3}$$

respectively, with $\boldsymbol{R}$, the position vector on the free surface, g the gravitational acceleration, z the vertical coordinate, p_f the free surface pressure, and ρ the water density. Along the

bottom boundary Γ_b, a no-flow condition is prescribed as, $\overline{\frac{\partial \phi}{\partial n}} = 0$. Various methods can be used for generating waves in the NWT. Here, we simulate piston wavemaker on boundary Γ_w, moving according to a prescribed motion, $x = x_w(t)$. Thus, we have, $\overline{\frac{\partial \phi}{\partial n}} = -\frac{\mathrm{d}x_w}{\mathrm{d}t}$, where the time derivative follows the wavemaker motion. Wavemaker laws are given later.

Prior to breaking, the steepness and asymmetry of periodic waves continuously increase during shoaling over a slope. This work focuses on sediment transport induced by such highly nonlinear and asymmetric waves. Wave overturning and breaking, which would interrupt NWT computations, are prevented by dissipating incident wave energy in a numerical Absorbing Beach (AB; Grilli and Horrillo 1997), located beyond the area of interest, for $x \geq x_a$ (Fig. 1). To create a negative work and absorb wave energy in the AB, an "absorbing" pressure term $p_f = p_a$ is specified in the dynamic free surface condition (3) (with $z = \eta$), proportional to the normal particle velocity. Additional wave reduction is induced by causing waves to de-shoal, using an AB bottom geometry similar to a natural bar. The pressure term is ramped-up following a $\tanh$ variation for $x_a \leq x \leq x_r$. An absorbing piston (AP; Grilli and Horrillo 1997) is also specified at the extremity of the AB, for $x = x_p$, which moves proportionally to the hydrodynamic pressure force caused by waves, calculated as a function of time in the NWT (see references for details). Grilli and Horrillo showed that the combination AB/AP effectively absorbs incident wave energy in the NWT, to within any specified value. For short distances of propagation over a smooth bottom, damping due to bottom friction is quite small, and is usually neglected in numerical models, even for long waves, when the computational domain only spans a few wavelengths (e.g., Grilli et al. 1994; Grilli et al. 1997). To simulate wave shoaling over a rippled sandy bed, which induces more significant damping due to bed roughness, Grilli et al. (2003) simulated an energy dissipation term due to bottom friction in the NWT. Here, we did not implement a moving sediment bed and, hence, neglected bottom friction effects on wave shape and velocities. Such effects could however be included in a later time.

The potential, and its normal- and time-derivatives $(\frac{\partial \phi}{\partial n}, \frac{\partial \phi}{\partial t}, \frac{\partial^2 \phi}{\partial t \partial n})$, are computed as a function of time in the NWT, along boundary Γ. The solution within domain Ω, can then be explicitly calculated based on the boundary solution. Internal velocity fields are required to initialize the NS-LES model and velocities, and their time derivative is also needed to calculate the wave-induced internal dynamic pressure gradient. If we denote by $\nabla_l \equiv (\partial/\partial x_l, \partial/\partial z_l)$ the gradient operator with respect to the coordinates of point $\boldsymbol{x}_l \in \Omega$, Eq. (1) yields,

$$\boldsymbol{u}(\boldsymbol{x}_l) = \int_\Gamma \left\{ \frac{\partial \phi}{\partial n} (\nabla_l G) - \phi \left(\nabla_l \frac{\partial G}{\partial n} \right) \right\} d\Gamma \tag{4}$$

where,

$$\nabla_l G = \frac{\boldsymbol{r}}{2\pi\, r^2} \quad ; \quad \nabla_l \left(\frac{\partial G}{\partial n} \right) = \frac{1}{2\pi\, r^2} \left\{ \boldsymbol{n} - 2\boldsymbol{r}\, \frac{\boldsymbol{r} \cdot \boldsymbol{n}}{r^2} \right\} \tag{5}$$

From Eq. (3), the wave-induced dynamic pressure gradient within Ω is expressed as,

$$\nabla_l p_D(\boldsymbol{x}_l) = -\rho \left\{ \frac{\partial \boldsymbol{u}}{\partial t} + \boldsymbol{u} \cdot \nabla_l \boldsymbol{u} \right\} \tag{6}$$

where the first term in the right-hand-side of Eq. (6) is obtained by expressing Eq. (4) for $(\frac{\partial \phi}{\partial t}, \frac{\partial^2 \phi}{\partial t \partial n})$, and the last term, by applying ∇_l to Eq. (4), which yields an equation similar to (4), expressed with the ∇_l of Eq. (5).

Numerical Methods used in NWT

The BIE (1) is solved by a BEM, at N discretization nodes on the boundary ($\boldsymbol{x}_l; l = 1 \ldots, N$), defining M higher-order elements to interpolate in between these. Here, we use quadratic isoparametric elements on lateral and bottom boundaries, and cubic elements ensuring continuity of the boundary slope on the free surface (Grilli and Subramanya 1996). Integrals are numerically calculated by Gauss integration. The Green's function and its normal derivative in Eq. (2) are singular as $r \to 0$. Special integrations methods are applied to singular terms (Grilli and Subramanya 1996). When applying Eq. (1) to points $\boldsymbol{x}_l$ that are very close to a different part of the boundary (e.g., near corners in Fig. 1), almost-singular integrals will occur when r is very small. The numerical accuracy of such integrals is improved with an adaptive integration method, in which boundary elements are subdivided into an increasingly large number of sub-segments, as a function of a distance-based algorithm. Integrals such as in Eq. (4), expressing interior fields, are non-singular and are evaluated by Gauss quadrature. However, for interior points located very close to boundary Γ, Similar to corner points in the discretized BIE (1), the integral kernels rapidly grow as r becomes small, yielding inaccurate numerical integration. These so-called quasi-singular integrals are also computed by adaptive integration (Grilli and Subramanya 1996).

Free surface boundary conditions (3) are time integrated based on explicit second-order Taylor series, for $\boldsymbol{R}$ and ϕ, expressed with time step Δt and Lagrangian time derivative, D/Dt. First-order coefficients in the series correspond to Eqs. (3), in which ϕ and $\frac{\partial \phi}{\partial n}$ are obtained from the solution of BIE (1) for at time t. Second-order coefficients are expressed as D/Dt of Eqs. (3) and calculated using the solution of a second similar BIE for ($\frac{\partial \phi}{\partial t}$, $\frac{\partial^2 \phi}{\partial t \partial n}$), for which boundary conditions are obtained from the solution of the first BIE and the time derivative of boundary conditions. The optimal Δt is adaptively set based on a mesh Courant number ($\simeq 0.45$; Grilli and Subramanya 1996).

Equations and Boundary Conditions for NS and sediment transport models

The equations governing fluid motion in domain $\Omega_{\rm LES}$ (Fig. 3a) are continuity and the volume-filtered incompressible Navier Stokes equations (with the Boussinesq approximation), and a source term for the wave forcing,

$$\frac{\partial \overline{u_i}}{\partial x_i} = 0 \quad ; \quad \frac{\partial \overline{u_i}}{\partial t} + \frac{\partial}{\partial x_j}\left(\overline{u_i}\,\overline{u_j} + \frac{\overline{p}}{\rho}\delta_{ij} - \nu \frac{\partial \overline{u_i}}{\partial x_j} + \tau_{ij} \right) = -\frac{1}{\rho}\frac{\partial p_D}{\partial x_i} \tag{7}$$

Here, u_i is the 3D velocity ($i = 1, 2, 3$), $\tau_{ij} = \overline{u_i u_j} - \overline{u_i}\,\overline{u_j}$ is the Sub-Filter Scale (SFS) shear stress term, $-\partial p_D/\partial x_i$ is the momentum source term for the forcing wave motion in the NWT, from Eq. (6), ν is the kinematic viscosity, x_i is the cartesian coordinate ($i = 2$ is vertical), and the overbars denote spatial filtering with a box filter. Here, because of the inherent mismatch between the irrotational NWT and rotational NS solutions, we elected to use one-way coupling by driving the NS solution with the full dynamic pressure from the NWT solution and have not forced the velocities at the NS domain boundary. The SFS term is represented by the Smagorinsky model, an eddy viscosity model which gives the local eddy viscosity ν_T as proportional to the magnitude of the local strain rate tensor (Zang et al. 1993). On the inflow/outflow boundaries and along the top of domain $\Omega_{\rm LES}$, we specify a gradient free condition: i.e., $\partial \overline{u_k}/\partial x_1 = 0$, and $\partial \overline{u_k}/\partial x_2 = 0$, respectively, where $k = 1, 2, 3$. The bottom boundary condition on Γ_b is no-slip, or $\overline{u_i} = 0$, implemented via the Immersed Boundary Method, described below. The lateral boundaries are treated as free slip surfaces, satisfying $\partial \overline{u_3}/\partial x_3 = 0$, $\partial \overline{u_1}/\partial x_3 = 0$, and $\overline{u_3} = 0$.

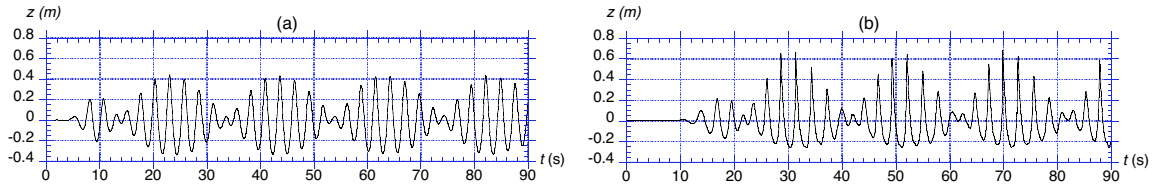

Fig. 4. Wave groups shoaling over a 1:20 slope in the NWT (domain similar to that of Fig. 1) : (a) deep water; (b) shallow water close to breaking.

The suspended sediment concentration in domain Ω_{LES} is modeled with a volume-filtered advection-diffusion equation,

$$\frac{\partial \overline{C}}{\partial t} + \frac{\partial}{\partial x_j}\left((\overline{u_j} - w_s \delta_{i2})\overline{C} + \chi_j \right) = 0 \tag{8}$$

where C = sediment concentration by volume fraction, $\chi_j = \overline{u_j C} - \overline{u_j}\,\overline{C}$ = SFS scalar flux term. For the inflow/outflow and top boundaries, we use gradient free boundary conditions. For the bottom boundary Γ_b, we use an empirical function developed by vanRijn (1984a) for evaluating the sediment concentration near the bed, as it varies along the bed.

Numerical Method used in NS and sediment transport models

The QUICK (Leonard 1979) algorithm is used for the spatial discretization of the advection terms in the momentum Eqs. (7), and central differences for all other terms. The same methods are used for discretizing the advection-diffusion for the sediment concentration field, except that SHARP (Leonard 1988) is used in place of QUICK, for its improved handling of sharp gradients. Both equations employ a Crank-Nicolson averaging for the diagonal viscous terms, and the Adams-Bashforth method for all other terms, which yields a semi-implicit, quasi-tridiagonal system of equations. This system of equations is solved with a fractional step method. Of the many versions of the code originally developed by Zang et al. (1994), we employ a modified version of the Tseng and Ferziger (2003) code, with an Immersed Boundary Method (IBM) implemented via a ghost cell method (Tseng and Ferziger 2003). The IBM works by applying the force necessary at the location of the immersed boundary to enforce the physical boundary condition, $\overline{u_i} = 0$ in this case.

APPLICATIONS

For the initial validation of our coupling methodology, we simply simulated periodic waves in the NWT to drive the NS-LES and sediment transport models. Incident waves, however, can be arbitrary. Fig. 4, for instance, shows an incident nonlinear wave group simulated in deep and shallow water in the NWT. The high asymmetry and nonlinearity of the waves is quite clear in Fig. 4b. Such more realistic wave forcing will be used in future simulations. We present results for both a flat bottom and a 75% buried cylinder. The NWT provides the far field velocities and free-surface wave forcing throughout most of domain Ω, while the embedded NS solution provides a well-resolved description of the wave boundary layer within domain Ω_{LES}, with no slip enforced at the bed (Fig. 3a). Results are qualitatively compared with those obtained for the forcing of the NS-LES and sediment transport models over a rippled bed by a simple oscillatory flow (Zedler and Street, 2001, 2002).

Discretization and Parameters

Typical free surface discretizations in the NWT (on Γ_f) usually have at least 20 nodes per dominant wavelength (Fig. 1). Lateral boundaries (Γ_w and Γ_p) are typically discretized with only 7-11 nodes. Bottom discretizations (on Γ_b) are usually a little coarser than on the free surface, but horizontal node spacing (Δx) is reduced on the bottom under the NS-LES domain $\Omega_{\rm LES}$, in order to further increase the accuracy of the integrals used to compute internal fields in the BEM solution. Adaptive integrations, with up to 2^4 subdivisions, are performed within 4 nodes of any corner of the BEM domain, and for all elements located directly under $\Omega_{\rm LES}$, where points at which internal velocities and pressure gradients are calculated and used for model coupling are specified. Initial time steps are selected based on the free surface node spacing, to satisfy the optimal mesh Courant number. Time step is subsequently automatically adjusted as a function of the minimum distance between nodes on the free surface in order to satisfy the Courant condition. Typical CPU times in the NWT are less than one second per time step on a desktop computer. Here, the NWT was run without bottom friction, and with no regridding applied on the free surface, because no long term computations were done in the NWT at this stage, since, for periodic waves, only one single representative period of wave forcing was used to force the NS-LES domain. Longer term computations, for instance with moving bed (such as migrating ripples), would require regridding the free surface (see Grilli et al. 2003; Grilli et al. 2004). An absorbing beach AB and an absorbing piston AP (Fig. 1) were specified in each case, in order to damp incident wave energy and eliminate wave reflection at the NWT extremity. The NS-LES model grid dimensions are 0.3 m long by 0.1727 m high by 0.0125 m wide. For the partially buried obstacle, the bottom is flat in the streamwise direction to either side of a central bump, represented by a 75% buried cylinder of radius 0.084 m, whose axis runs in the spanwise direction. The NS-LES model is discretized by 82 x 98 x6 grid points. Hence, we use 82x98 = 8,036 points in each vertical plane of the 3D NS-LES domain. With so few gridpoints in the spanwise direction, however, these are effectively 2D simulations. The immersed boundary is located above the actual grid boundary so that the total flow domain height is 0.17 m (discretized by 95 points in the vertical direction over the flat regions). Here, we assume the sediment is quartzy sand (sediment density: $2,650$ kg/m^3), with a particle size $d_{50} = 200\,\mu$m.

Wave generation in the NWT is ramped-up over three periods and computations are performed until a quasi-steady regime is reached. This usually takes 10 wave periods or so. Internal velocity fields are then calculated in the NWT, to initialize the NS-LES model over a grid of points within the small immersed domain $\Omega_{\rm LES}$ (e.g., Fig. 3a). Pressure gradient fields are calculated over the same grid for later time steps, to provide the Momentum Source term in the NS-LES model Eq. (7). Thus, the NWT forcing is applied at each grid point of the NS-LES model, in the horizontal and vertical momentum equations, and varies downstream, vertically, and in time. Internal fields computed in the 2D-NWT, for grid points in the vertical plane, are then copied uniformly to each vertical grid in the third dimension of the 3D NS-LES domain. Initial velocities are thus assumed 2D when passed from the NWT to the NS-LES model, i.e., with $u_3 = 0$, and for later time steps, internal pressure gradients forcing the NS-LES model are also assumed 2D, with $\partial p_D/\partial x_3 = 0$. Note, for periodic waves, only a wave period worth of forcing fields is computed and used in a loop to force the NS-LES model computations over many subsequent periods.

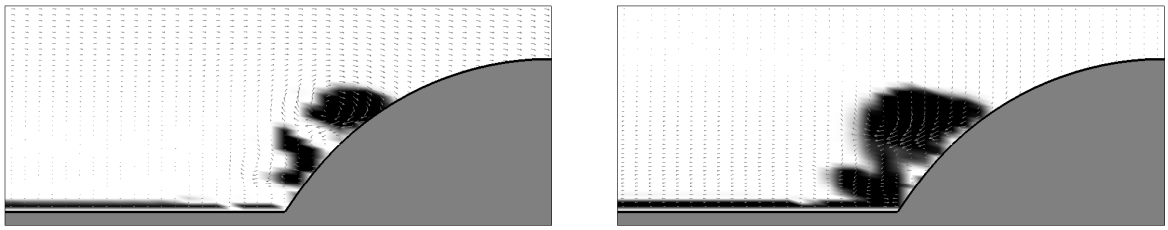

Fig. 5. Case of Fig. 3: Sediment concentration (gray scale) and (u, v) velocity, on the centerplane of NS-LES domain, Flow direction: (a-left) to right; (b-right) to left.

Periodic Wave Flow Over a Partly Buried Cylinder

We specify a periodic wave of period $T = 2.94$ s and incident height $H_o = 0.12$ m in the NWT. To validate the coupling of the irrotational NWT flow with the full NS solution, we compare the wave-induced velocities in the NWT to those computed in the NS-LES model, when forced by the NWT pressure gradient fields, during the first period of run time. Fig. 3b shows velocity components at the upper left corner of the NS-LES grid of Fig. 3a. Velocities in both models agree reasonably well at this time. For later times, however, this agreement deteriorates (results not shown here), likely because we force the NS-LES simulations by repeating the NWT data periodically, which is not strictly accurate for nonlinear waves. This causes a slight phase shift, which becomes gradually more pronounced after the initial run period. Both detailed velocity and sediment concentration results are shown in Fig. 5, for two times selected during the eleventh period of run time (the first 10 periods are model ramp-up). The suspended sediment concentration field was initialized as a function of the bottom shear stress at the end of the tenth period. Bedload was not computed for this initial illustration, and we also artificially caused sediment entrainment during most of the flow period, at most locations along the bed.

Characteristic of all boundary layers, velocity profiles tend to zero along the bed, with larger near-bed velocities surrounding the crest of the cylinder. This is consistent with observations that the highest shear stresses over ripples occur either just upstream (Zedler and Street 2005) or at the ripple crest (Sleath 1982). Similar to the findings of (Zedler and Street 2002) for a uniform oscillatory flow over sinusoidal ripples, shear layers form in the lee of the mine during wave phases where the velocity tapers off from its maximum value. As shown in Fig. 5, the boundary layer development around the buried cylinder differs considerably from that which forms in the pure oscillatory flow case around ripples, as in Zedler and Street (2005). It is thought that the main differences are due to the phasing and spatial distribution of the forcing demonstrated in the NWT, as compared with the spatially-uniform, purely time-dependent, forcing of the oscillatory flow case. The major observed difference here is that a spanwise vortex forms on the *stoss* slope of the mine, every half period, whereas a spanwise vortex would normally form in the lee of the mine (or ripple) in a pure oscillatory flow case. The observed sediment transport dynamics are qualitatively similar to previous simulations with the NS-LES model by Zedler and Street (2005), in that they are heavily guided by the boundary layer motions. In general, sediment is picked up where the shear stresses are greater than critical along the flat bottom regions both upstream and downstream of the mine. The entrained plumes then oscillate over the cylinder due to the action of the flow aloft. Of particular interest, we find that the stoss vortex, which forms every half cycle, acts to trap previously entrained sediment, which flows past it, as the velocity tapers off

from its maximum value. Strictly, these results are only a first approximation to the correct boundary condition, which would allow for sediment deposition and subsequent pickup on the obstacle boundary Γ_b, such as does the flux condition of Celik and Rodi (1991).

CONCLUSIONS

The coupling between the NWT and the NS-LES model to simulate wave induced sediment transport has produced interesting boundary layer dynamics under a realistic orbital wave motion. The main conclusions are: (i) our approach successfully produces a nonlinear orbital wave-like flow in the NS-LES model; (ii) the boundary layer motions around the partially buried cylinder differ considerably between the wave and pure oscillatory flow cases, and as well with those which typically form around ripples in oscillatory flows; (iii) the sediment transport dynamics are qualitatively similar to previous simulations with the NS-LES model in that they are heavily guided by the boundary layer motions. Cases with a sloping bathymetry will be reported on in future work as well as cases of sediment transport forced by more complex shoaling wave fields. No moving bed algorithm was yet implemented in the models, which would allow simulating wave-induced ripple formation and migration or scouring/burial near bottom obstacles. Our modeling approach affords this capability and the addition of a moving bottom is ongoing work.

ACKNOWLEDGEMENTS

Support from Grants N00014-00-1-0440 and N00014-05-1-0068 (ONR Coastal Dynamics Program, code 321CG, Dr. Thomas Drake, Program Officer) is gratefully acknowledged. A grant of computer time was provided by the DOD High Performance Computing Modernization Program.

REFERENCES

Barr, B., Slinn, D., Pierro, T., and Winters, K. (2004). "Modeling unsteady turbulent flows over ripples : Reynolds-averaged navier-stokes equations (rans) versus large-eddy simulation (les).." *J. of Geophysical Research*, 109(C09009), 1–19.

Biausser, B., Grilli, S. T., Fraunie, P., and Marcer, R. (2004). "Numerical analysis of the internal kinematics and dynamics of three-dimensional breaking waves on slopes." *Intl. J. Offshore and Polar Engng.*, 14(4), 247–256.

Celik, I. and Rodi, W. (1991). "Suspended sediment transport capacity for open channel flows.." *Journal of Hydraulic Engineering*, 128(12), 1051–1059.

Chang, Y. and Scotti, A. (1991). "Numerical simulation of turbulent, oscillatory flow over sand ripples.." *J. of Geophysical Research*, 109(C09012), 1–16.

Grilli, S. T. and Horrillo, J. (1997). "Numerical generation and absorption of fully nonlinear periodic waves." *J. Engng. Mech.*, 123(10), 1060–1069.

Grilli, S. T. and Horrillo, J. (1999). "Shoaling of periodic waves over barred-beaches in a fully nonlinear numerical wave tank." *Intl. J. Offshore and Polar Engrg.*, 9(4), 257–263.

Grilli, S. T. and Subramanya, R. (1996). "Numerical modeling of wave breaking induced by fixed or moving boundaries." *Computational Mech.*, 17, 374–391.

Grilli, S. T., Subramanya, R., Svendsen, I. A., and Veeramony, J. (1994). "Shoaling of solitary waves on plane beaches." *J. Waterway Port Coastal and Ocean Engng.*, 120(6), 609–628.

Grilli, S. T., Svendsen, I. A., and Subramanya, R. (1997). "Breaking criterion and characteristics for solitary waves on slopes." *J. Waterway Port Coastal and Ocean Engng.*, 123(3), 102–112.

Grilli, S. T., Voropayev, S., Testik, F. Y., and Fernando, H. J. S. (2003). "Numerical modeling and experiments of wave shoaling over buried cylinders in sandy bottom." *Proc. 13th Offshore and Polar Engng. Conf.*, Honolulu, Hawaii. 405–412.

Grilli, S. T., Voropayev, S., Testik, F. Y., and Fernando, H. J. S. (2004). "Numerical modeling and experiments of periodic waves shoaling over semi-buried cylinders in sandy bottom." *J. Waterways Port Coastal and Ocean Engrg.* (in revision).

Guignard, S., Grilli, S. T., Marcer, R., and Rey, V. (1999). "Computation of shoaling and breaking waves in nearshore areas by the coupling of BEM and VOF methods." *Proc. 9th Offshore and Polar Engng. Conf.*, Vol. III, ISOPE99, Brest, France. 304–309.

Leonard, B. P. (1979). "A stable and accurate convective modelling procedure based on quadratic upstream interpolation.." *Computer Methods in Applied Mechanics and Engineering*, 19(1), 59 – 98.

Leonard, B. P. (1988). "Simple high accuracy resolution program for convective modeling of discontinuities." *International journal for Numerical Methods in Fluids*, 8, 1291–1318.

Sleath, J. F. A. (1982). "The suspension of sand by waves." *Journal of Hydraulic Research*, 20(5), 439–452.

Tseng, Y. H. and Ferziger, J. H. (2003). "A ghost-cell immersed boundary method for flow in complex geometry." *Journal of Computational Physics*, 192(2), 593 – 623.

vanRijn, L. C. (1984a). "Sediment transport .1. bed-load transport." *Journal of Hydraulic Engineering*, 110(10), 1431–1456.

vanRijn, L. C. (1984b). "Sediment transport .3. bed forms and alluvial roughness." *Journal of Hydraulic Engineering*, 110(12), 1733–1754.

Voropayev, S. I., McEachern, G. B., Boyer, D. L., and Fernando, H. J. S. (1999). "Dynamics of sand ripples and burial/scouring of cobbles in oscillatory flow." *Applied Ocean Research*, 21(5), 249–261.

Voropayev, S. I., Testik, F. Y., Fernando, H. J. S., and Boyer, D. L. (2003a). "Burial and scour around short cylinder under progressive shoaling waves." *Ocean Engineering*, 30(13), 1647–1667.

Voropayev, S. I., Testik, F. Y., Fernando, H. J. S., and Boyer, D. L. (2003b). "Morphodynamics and cobbles behavior in and near the surf zone." *Ocean Engineering*, 30(14), 1741–1764.

Zang, Y., Street, R. L., and Koseff, J. R. (1993). "A dynamic mixed subgrid-scale model and its application to turbulent recirculating-flows." *Physics of Fluids A-Fluid Dynamics*, 5(12), 3186–3196.

Zang, Y., Street, R. L., and Koseff, J. R. (1994). "a non-staggered grid, fractional step method for time-dependent incompressible Navier Stokes equations in curvilinear coordinates." *Journal of Computational Physics*, 114(1), 18–33.

Zedler, E. A. and Street, R. L. (2001). "Large-Eddy Simulation of sediment transport: Currents over ripples." *J. of Hydraulic Engineering*, 127(6), 444–452.

Zedler, E. A. and Street, R. L. (2002). "Nearshore sediment transport processes: unearthed by Large-Eddy Simulation." *28th International Conference on Coastal Engineering*, J. M. Smith, ed. ASCE, 2504–2416.

Zedler, E. A. and Street, R. L. (2005). "Sediment transport over ripples in oscillatory flow." *J. of Hydraulic Engineering*. (in press).